

Phase-resolved real-time forecasting of three-dimensional ocean waves via machine learning and wave tank experiments

Rui Li ^a, Jincheng Zhang ^a, Xiaowei Zhao ^{a,*}, Daming Wang ^b, Martyn Hann ^b, Deborah Greaves ^b

^a Intelligent Control & Smart Energy (ICSE) Research Group, School of Engineering, University of Warwick, Coventry, UK

^b School of Engineering, Computing and Mathematics, University of Plymouth, Plymouth, UK

ARTICLE INFO

Keywords:

3D waves
Convolutional neural network
Machine learning
Multilayer perceptron
Phased-resolved wave forecasting
Wave tank experiments

ABSTRACT

Accurate prediction of ocean waves plays an essential role in many ocean engineering applications, such as the control of wave energy converters and floating wind turbines. However, existing studies on phase-resolved wave prediction using machine learning mainly focus on two-dimensional wave data, while ocean waves are usually three-dimensional. In this work, we investigate, for the first time, the phase-resolved real-time prediction of three-dimensional waves using machine learning methods. Specifically, the wave prediction is modeled as a supervised learning task aiming at learning mapping relationships between the input historical wave data and the output future wave elevations. Four frequently-used machine learning methods are employed to tackle this task and a novel Dual-Branch Network (DBNet) is proposed for performance improvement. A group of wave basin experiments with nine directional wave spectra under three sea states are first conducted to collect the data of 3D waves. Then the wave data are used for verifying the effectiveness of the machine learning methods. The results demonstrate that the upstream wave data measured by the gauge array can be used for control-oriented wave forecasting with a forecasting horizon of more than 20 s, where the directional information provided by the upstream gauge array is vital for accurately predicting the downstream wave elevations. In addition, further investigations show that by using only local wave data (which can be easily obtained), the very short-term phase-resolved prediction (less than 5 s) can be achieved.

1. Introduction

As one of the main renewable energy sources, wave energy is an important and promising low-carbon alternative to fossil fuels. Although many kinds of Wave Energy Converters (WECs) have been designed and verified [1,2], when compared to solar and wind energy, wave energy is still far from being commercially competitive [3]. One major challenge in further reducing the cost of wave energy is the design of a control technique suitable for various sea states. To improve the control performance, the preview-based hydrodynamic control [4–6] has been proposed where the controller is designed to react in advance before the waves hit the WEC structures. It can significantly enhance the power generation of WECs [7]. For example, the investigation of an Azura WEC under experimental conditions showed that a 36% improvement in power generation could be achieved by the Model Predictive Control (MPC) compared with the standard fixed damping control [8]. However, the WEC control is a non-causal optimal control problem [9] where the current control decision must be based on

the future wave excitation force [6]. Thus, the real-time forecasting of the wave information is essential for executing energy-maximizing controllers [10]. A feasible and promising scheme to obtain the future wave excitation force is to compute it from wave elevation predictions [11,12]. Indeed, as an essential technology in WEC control design, wave elevation prediction has drawn a lot of attention and has now become an active research area.

Based on the spectral transport and energy balance equations, the traditional phase-averaged wave forecasting method aims at predicting the wave spectrum instead of the wave profile shape [13]. The frequently-used third-generation models such as WAVEWATCH III [14], SWAN [15] and WAM [16] can provide statistical quantities, such as sea states defined by 1-hour or 3-hour statistics, including the significant wave height (H_s), the peak spectral wave period (T_p) and the mean wave direction [17]. Although meaningful guidance for the WEC design can be derived from these works, they cannot be used in real-time WEC control applications as the phase-resolved wave elevation is unavailable [18].

* Corresponding author.

E-mail addresses: rui.li.4@warwick.ac.uk (R. Li), jincheng.zhang.1@warwick.ac.uk (J. Zhang), xiaowei.zhao@warwick.ac.uk (X. Zhao), daming.wang@plymouth.ac.uk (D. Wang), martyn.hann@plymouth.ac.uk (M. Hann), deborah.greaves@plymouth.ac.uk (D. Greaves).

Nomenclature	
Abbreviations	
2D	Two-Directional
3D	Three-Directional
ANN	Artificial Neural Network
BN	Batch Normalization
BNN	Bayesian Neural Network
CBR	CNN + BN + ReLU
CNN	Convolutional Neural Network
CRNN	Convolutional Recurrent Neural Network
DBNet	Dual-Branch Network
GRU	Gated Recurrent Unit
HF	High Frequency
HOS	Higher-Order Spectral
LSTM	Long Short-Term Memory
MAE	Mean Absolute Error
ML	Machine Learning
MLP	Multilayer Perceptron
MPC	Model Predictive Control
NLS	Non-Linear Schrödinger
ReLU	Rectified Linear Unit
RNN	Recurrent Neural Network
RMSE	Root Mean Square Error
SCRTP	Scientific Computing Research Technology Platform
SVM	Support Vector Machines
WEC	Wave Energy Converter
WG	Wave Gauge
Symbols	
E	The expected loss
\mathcal{F}	The ML model
H_s	The significant wave height
I	The whole number of predictions in the training set
l	The historical time steps for the input
\mathcal{L}	The loss function
m	The predicted time horizon using local wave information
N	The whole number of predictions in the test set
n	The predicted time horizon using upstream wave information
T	The current time step
T_p	The peak spectral wave period
\mathcal{U}_F	The reference future wave elevations measured by wave gauges
$\hat{\mathcal{U}}_F$	The approximate future wave elevations predicted by ML models
\mathcal{U}_H	The input historical wave information measured by wave gauges
$\hat{\mathcal{U}}_{T+1:T+m}^4$	The approximate future wave elevation of WG4 predicted by the ML model from time steps $T+1$ to $T+m$
$\mathcal{U}_{T-l:T}^4$	The historical wave information measured by WG4 from time steps $T-l$ to T
$\mathcal{U}_{T-l:T}^{2,5,6,7,8}$	The historical wave information measured by WG2, WG5, WG6, WG7 and WG8 from time steps $T-l$ to T
\hat{u}_{T+n}^4	The approximate wave elevation of WG4 predicted by the ML model at time step $T+n$
u_{T-l}^4	The wave elevation measured by WG4 at time step $T-l$
$u_{T-l}^{2,5,6,7,8}$	The wave elevation measured by WG2, WG5, WG6, WG7 and WG8 at time step $T-l$
λ	The tradeoff parameter of $\Phi(\cdot)$
θ	The parameters of the ML model
Φ	The regularization term

The phase-resolved wave model has drawn more and more attention in recent years, which is of particular interest for the preview-based control of WECs [19]. To significantly enhance the performance of the WEC controllers, a forecast with at least a 20 s time horizon is usually required [20]. However, achieving an accurate prediction for such a long-time horizon is exceptionally challenging, which has become one of two essential barriers in practical applications for WEC control (the other barrier is the physical implementation of the control system) [21]. Although the models [22,23] based on linear wave theory can forecast the downstream wave elevation from the upstream information in real-time, they are only effective for the very short-term prediction and are limited to the sea states with small steepness [17]. Thus, more and more non-linear approaches such as Higher-Order Spectral (HOS) methods have been proposed in recent years [24,25]. For example, a novel wave forecast model coupling ensemble Kalman filter and HOS method was proposed in [24] and enhanced in [26] by simultaneously estimating the ocean current field. In practice, restricted by the intensive computational requirement of HOS, the reduced order or approximate equations are usually considered efficient alternatives [19]. For example, many prediction models are based on the model equations, such as the weakly Non-Linear Schrödinger (NLS) models [27,28]. Typically, the high-order NLS equation is an order faster than the HOS method but is less accurate, as the former normally assumes a narrow-banded wave field and small steepness [28].

Recently, Machine Learning (ML), a data-driven method, has shown great potential in automatically capturing non-linear and hierarchical features. A series of ML-based studies have been conducted to predict the statistical wave characteristics such as the significant wave height [29–31], peak spectral wave period [32–34] and wave speed [35]. The machine learning method has also been applied to phase-resolved wave forecasting. For example, in [19], a Convolutional Recurrent Neural Network (CRNN) was proposed to predict non-linear dispersive non-breaking wave evolution including rogue waves. The Artificial Neural Network (ANN) was adopted by [17] for unidirectional wave prediction. The ANN model was also applied in long-crest wave prediction [18] and verified under unknown sea states [36]. Two forecast algorithms, including an ML-based Support Vector Machines (SVM) regression, were used in [37] to forecast wave elevations and wave excitation forces, which were then applied for feed-forward control of offshore floating wind turbines. The Bayesian Neural Network (BNN) was also introduced and applied to phase-resolved real-time wave prediction in [38], where both the aleatory and epistemic uncertainties were thoroughly investigated. However, two critical limitations hugely reduce their practical value in engineering applications. First, a single model cannot handle different sea states. For example, in [18], four ANN models were trained respectively for four different sea states (i.e. sea state 4–7) and then used to forecast the corresponding wave elevations. When generalizing a trained model to an unknown sea state, the error would surge significantly (about 6 to 11 times compared to the trained sea state) [36]. In [19], the performance of their CRNN was only verified by sea state 6. Three ANN models were trained for three different wave conditions in [39] based on simulated multi-directional waves. Obviously, a universal model that can cope with different sea

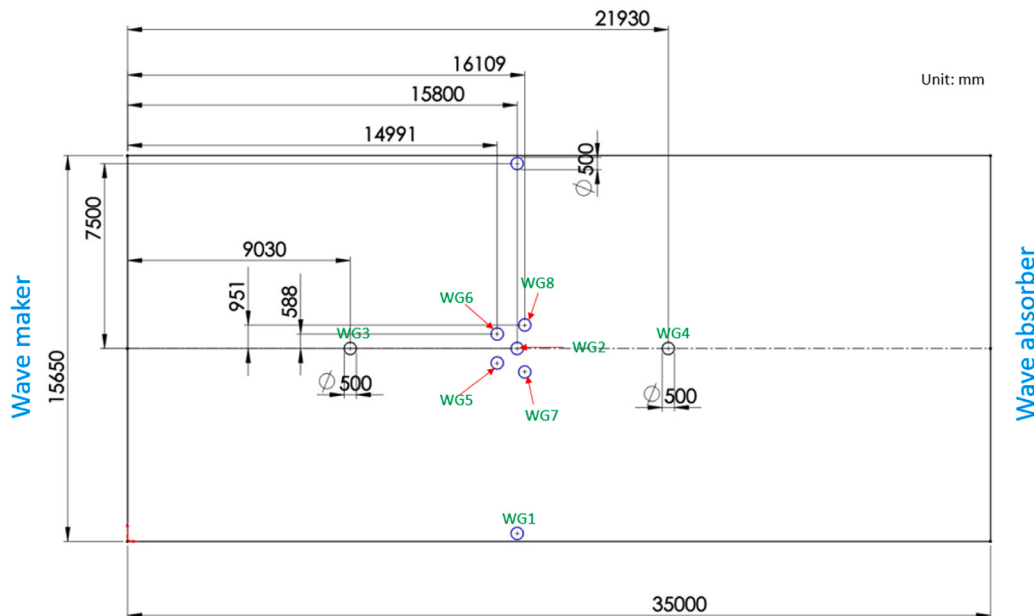


Fig. 1. The layout of the wave basin experiments, where WG2, WG5, WG6, WG7 and WG8 constitute the pentagonal gauge array.

Table 1

The comparison of the proposed wave forecasting method with existing methods in the literature, where Multiple means multiple models are trained for different sea states and Universal means a single universal model is trained for different sea states.

Reference	Main contribution	Wave and model features		
		Data generation	Wave dimensions	Model
[18]	An ANN-WP model for prediction	Tank experiments	2D	Multiple
[36]	The ANN-WP for unknown sea states	Tank experiments	2D	Multiple
[37]	Wave prediction for control	Tank experiments	2D	Multiple
[19]	A CRNN model for prediction	Numerical simulations	2D	Multiple
[39]	An ANN model for prediction	Numerical simulations	2D & 3D	Multiple
[17]	An ANN model for prediction	Numerical simulations	2D	Universal
[38]	The evaluation of prediction uncertainty	Tank experiments	2D	Universal
This work	A DBNet model for 3D wave prediction	Tank experiments	3D	Universal

states is better than multiple models for different scenarios, as the latter is not only time-consuming but also error-prone. Second, the existing ML-based phase-resolved forecasting works still mainly focus on unidirectional waves, such as [17,37]. In practice, ocean waves are usually three-dimensional (3D) except for near-shore areas where waves align due to shoaling [40]. Thus, the prediction of 3D ocean waves needs great attention.

As shown in Table 1, the existing phase-resolved wave forecasting methods based on deep learning mainly focus on 2D wave data, where the only research involving 3D wave [39] is still based on simulation data instead of more realistic tank experiments. Moreover, most deep learning models for wave forecasting can only handle a single sea state, while different sea states need multiple and separately-trained models to predict. This issue seriously limits their practical use as the model will need a pre-processing procedure to identify the state of the input historical wave data. If the sea state was wrongly classified or the input data was not enough to be distinguished, then the prediction accuracy would be very low as the adopted model would not match the sea state (about 6 to 11 times lower compared to the matched model for 2D waves [36]). To overcome the above limitations of existing works, this paper employs four ML-based methods and proposes a novel Dual-Branch Network (DBNet) for the phase-resolved forecasting of 3D waves, where the ML models are designed to handle multiple sea states simultaneously. To be specific, in this work, a group of wave basin experiments is conducted first, where nine different directional wave spectra under three sea states are generated. Then, four frequently-used ML-based methods, including Gated Recurrent

Unit (GRU) network, Long Short-Term Memory (LSTM) network, Multi-layer Perceptron (MLP) and Convolutional Neural Network (CNN), are trained and adopted to forecast the wave elevation for all nine wave conditions under three sea states without retraining multiple times. Further, by combining the advantages of both MLP and CNN, a novel DBNet is proposed with an MLP-based branch and a CNN-based branch for wave prediction, which can predict future wave elevation with better performance than the other four ML-based methods. As far as we know, this work is the first attempt to apply machine learning for the phase-resolved real-time forecasting of 3D waves based on wave tank experiments. The results of the experimental data show that the relative Root Mean Square Error (RMSE) of the proposed DBNet is about 11.6% normalized by the significant wave height (averaged for nine wave conditions), which is much better than the scheme for unidirectional wave prediction in [36] (where the problem itself is easier than the prediction of 3D waves) which generalizes a trained model to unknown sea states (14.7% on average). The main contributions and novelties of this paper are summarized as follows:

- (1) The phase-resolved real-time forecasting of 3D waves using machine learning methods is comprehensively investigated. Two major limitations of existing works that significantly hinder the potential of ML-based wave prediction, i.e. the generalization of the model to diverse sea states and the prediction of 3D waves (the existing works based on ML and wave tank experiments are all on 2D waves), are both tackled in this paper. The comparison of the proposed wave forecasting method with existing methods in the literature is summarized in Table 1.

- (2) The performance of four frequently-used machine learning methods, including GRU, LSTM, MLP and CNN, are investigated and verified for the phase-resolved forecasting of 3D waves. Moreover, a novel DBNet is proposed to further enhance the accuracy of ML-based methods which can take advantage of both MLP and CNN.
- (3) A series of wave tank experiments are conducted with nine different directional wave spectra under three sea states. The above five ML-based phase-resolved prediction models are then trained, validated and tested to learn the mapping relationships between the input historical wave data and the output future wave elevations.
- (4) Two types of input historical wave data are studied for predictions of 3D waves, i.e. the upstream wave information measured by the gauge array and the local wave information measured by a single gauge. The quantitative results show that the former can enable the model to achieve control-oriented phase-resolved prediction (more than 20 s), while the latter can achieve very short-term prediction (less than 5 s). Moreover, the significance of the directional information for phase-resolved forecasting is also demonstrated.

The remaining part of this paper is organized as follows: the wave basin experiments, the problem formalization and the ML-based models are described in Section 2. The results are reported and discussed in Section 3. The conclusions are finally drawn in Section 4.

2. Methodology

2.1. Wave basin experiments

The wave basin experiments are conducted according to the characteristics of the WaveHub test site located 16 km offshore from Hayle on the north coast of Cornwall at the eastern edge of the Atlantic Ocean with an average water depth of 50 m. Two High Frequency (HF) radars are installed to cover the same ocean area to obtain the directional information of waves which collect 3161 hourly high-quality directional wave spectra from April 2nd, 2012 to December 4th, 2012. Then, the *K*-means clustering technique is employed to obtain a small number of conditions that can represent the characteristics of the measured ocean area, where nine typical conditions clustered in three groups are eventually determined. Based on the *K*-means clustering results, those nine representative conditions are then divided into three corresponding groups (one, three and five spectrum/spectra in each group, respectively). After that, the corresponding wave basin experiments are carried out based on the representative conditions.

As shown in Fig. 1, eight Wave Gauges (WGs) are mounted in the basin to measure the wave elevation. Nine representative directional wave spectra are created using a single summation method, which means each frequency component has a unique wave direction. Based on MATLAB, the wave creation files for different wave cases are created by defining the wave amplitude, direction and phase angle with corresponding frequency components. Before the creation of the input file, each directional wave spectrum is adjusted to guarantee that the dominant wave direction is the same as the wave maker direction. The scale ratio of the wave is 1:25 and the repeat time for the directional wave generation is 45 min (3.75 h in full scale with a scaling factor of $\sqrt{25}$ using the Froude scaling law). For each condition, about 3.5×10^5 points are sampled. The measured values of the significant wave height (H_s) and the peak spectral wave period (T_p) of each directional spectrum are shown in Table 2.

Table 2

The measured H_s and T_p of nine directional wave spectra, which have been transformed to the full scale.

Group	Wave condition	Sea state	H_s (m)	T_p (s)
1	1	4	1.875	8.845
	2	5	2.550	8.930
	3	5	4.000	9.890
	4	4	1.400	8.310
2	5	4	1.325	8.385
	6	5	3.375	9.575
	7	6	4.775	10.565
	8	5	3.300	8.645
3	9	4	2.300	8.655

2.2. Problem formalization

Two different types of inputs, i.e. the historical wave information measured by the upstream gauge array and by the local gauge, are investigated for the phase-resolved forecasting of 3D waves, which are illustrated in Fig. 2.

For the first scenario, as shown in Fig. 2(a), the historical upstream wave information from time steps $T - l$ to T measured by the WG2, WG5, WG6, WG7 and WG8 is selected as the input, while the downstream future wave elevation from time steps $T + 1$ to $T + n$ measured by WG4 is chosen as the output. Then, the target of an ML-based model is to predict the future wave elevation, i.e. from \hat{u}_{T+1}^4 to \hat{u}_{T+n}^4 based on the historical upstream wave information, i.e. from $u_{T-l:T}^{2,5,6,7,8}$ to $u_T^{2,5,6,7,8}$, which can be expressed as:

$$\begin{aligned}\hat{\mathcal{U}}_{T+1:T+n}^4 &= \mathcal{F}(\mathcal{U}_{T-l:T}^{2,5,6,7,8}; \theta), \\ \hat{u}_{T+1:T+n}^4 &= (\hat{u}_{T+1}^4, \hat{u}_{T+2}^4, \dots, \hat{u}_{T+n}^4), \\ \mathcal{U}_{T-l:T}^{2,5,6,7,8} &= (u_{T-l}^{2,5,6,7,8}, u_{T-l+1}^{2,5,6,7,8}, \dots, u_T^{2,5,6,7,8})\end{aligned}\quad (1)$$

where \mathcal{F} is the ML-based model and θ represents the parameters of \mathcal{F} . l means the historical time steps and n indicates the predicted future time steps. $\hat{u}_{T+1:T+n}^4$ represents the future wave elevation of WG4 predicted by the ML model from time steps $T + 1$ to $T + n$, while $\mathcal{U}_{T-l:T}^{2,5,6,7,8}$ denotes the historical wave information measured by WG2, WG5, WG6, WG7 and WG8 from time steps $T - l$ to T .

For the second scenario, as shown in Fig. 2(b), the historical local wave information from time steps $T - l$ to T measured by the WG4 itself is selected as the input, while the future wave elevation from time steps $T + 1$ to $T + m$ measured by WG4 is chosen as the output. Then, the target of an ML-based model is to predict the future wave elevation, i.e. from \hat{u}_{T+1}^4 to \hat{u}_{T+m}^4 based on the historical local wave information, i.e. from u_{T-l}^4 to u_T^4 , which can be expressed as:

$$\begin{aligned}\hat{\mathcal{U}}_{T+1:T+m}^4 &= \mathcal{F}(\mathcal{U}_{T-l:T}^4; \theta), \\ \hat{u}_{T+1:T+m}^4 &= (\hat{u}_{T+1}^4, \hat{u}_{T+2}^4, \dots, \hat{u}_{T+m}^4), \\ \mathcal{U}_{T-l:T}^4 &= (u_{T-l}^4, u_{T-l+1}^4, \dots, u_T^4)\end{aligned}\quad (2)$$

where m indicates the predicted future time steps. $\hat{u}_{T+1:T+m}^4$ represents the future wave elevation of WG4 predicted by the ML model from time steps $T + 1$ to $T + m$, while $\mathcal{U}_{T-l:T}^4$ denotes the local historical wave information measured by WG4 itself from time steps $T - l$ to T .

Hence, given an ML-based model \mathcal{F} , the target is to narrow the gap between the predicted wave elevation approximation and the real measured wave elevation as closely as possible by optimizing the parameters θ :

$$\begin{aligned}\theta^* &= \arg \min_{\theta} E(\theta), \\ E(\theta) &= \sum_{i=1}^I \mathcal{L}(\mathcal{U}_F, \hat{\mathcal{U}}_F) + \lambda \Phi(\theta), \\ \mathcal{L}(\mathcal{U}_F, \hat{\mathcal{U}}_F) &= \mathcal{L}(\mathcal{U}_F, \mathcal{F}(\mathcal{U}_H; \theta)),\end{aligned}\quad (3)$$

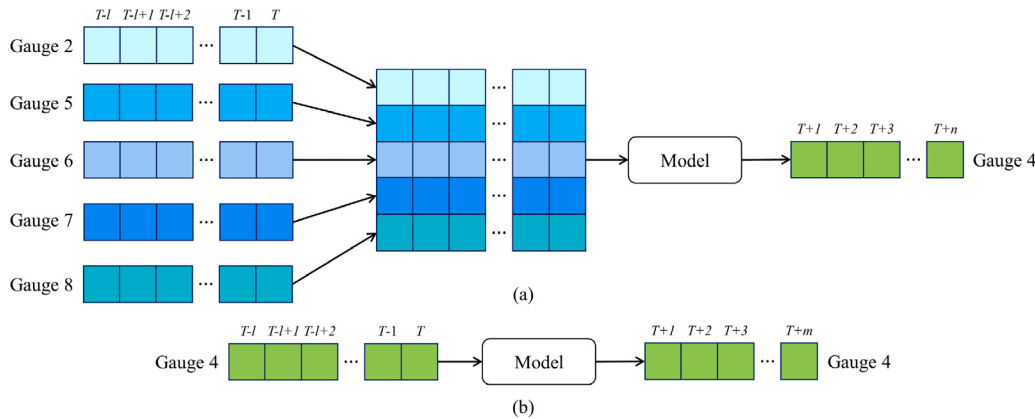


Fig. 2. The phase-resolved real-time forecasting of 3D waves using (a) the wave information measured by the upstream gauge array and (b) the wave information measured by the local gauge.

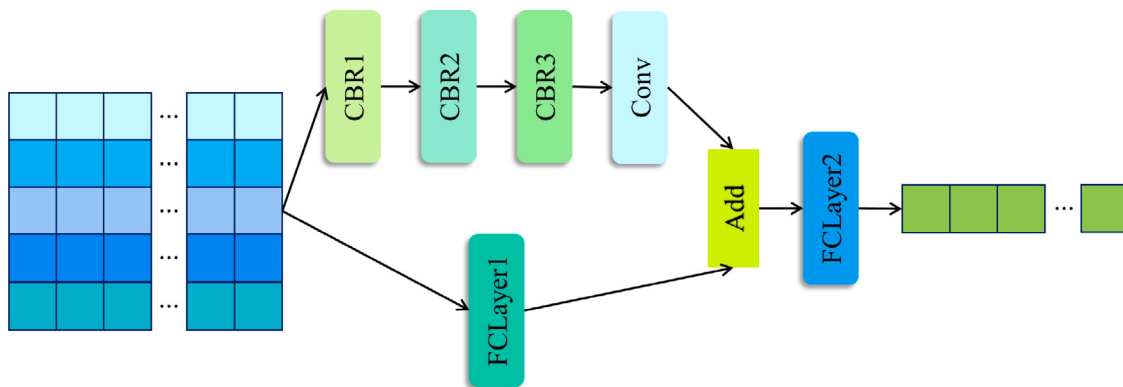


Fig. 3. The structure of the proposed DBNet, where FCLayer means the fully connected layer and CBR represents the convolutional layer with the BN operation and the ReLU activation function.

where \mathcal{U}_F and $\hat{\mathcal{U}}_F$ represent the future wave elevations measured by the gauge and predicted by the ML model, while \mathcal{U}_H means the input historical wave information. $E(\theta)$ indicates the expected loss, where the loss function $\mathcal{L}(\mathcal{U}_F, \hat{\mathcal{U}}_F)$ measures the disparity between the real measured and predicted wave elevation and $\Phi(\theta)$ is the regularization term weighted by the trade-off parameter λ . I represents the whole number of predictions in the training set.

2.3. Machine learning methods

As illustrated in Section 2.2, the input and output of the phase-resolved wave forecasting are both time-series wave elevations, which can be naturally modeled as a sequence-to-sequence problem from the machine learning perspective [41,42]. Therefore, four frequently-used sequence-to-sequence models, i.e. GRU, LSTM, MLP and CNN, are employed for resolving the wave forecasting problem. Meanwhile, to further improve the accuracy, a novel DBNet is proposed which combines the advantages of MLP and CNN.

2.3.1. LSTM and GRU

LSTM and GRU are two typical Recurrent Neural Networks (RNNs), while RNNs are designed to address sequential data with temporal dependencies such as text, audio and video. The LSTM is proposed to overcome the short-term memory problem of RNN [43]. An additional memory cell is equipped to store the information and three gates,

Table 3

The detailed setting of each layer in the DBNet where the wave elevations measured by the upstream gauge array are used as input.

Name	Input size	Output size	Channel	Kernel	Stride	Padding
CBR	Conv	1 × 5 × 300	4	(3, 7)	(1, 1)	(1, 3)
	BN	4 × 5 × 300	4	–	–	–
	ReLU	4 × 5 × 300	4	–	–	–
Conv	4 × 5 × 300	1 × 300	1	(5, 3)	(1, 1)	(0, 1)
FCLayer1	1 × 5 × 300	1 × 300	–	–	–	–
FCLayer2	1 × 300	1 × 85	–	–	–	–

i.e. input gate, output gate and forget gate, are designed to control the inside state of the LSTM cell. As a simple variant of LSTM, GRU only has two gates, named the update gate and the reset gate [44]. Without any extra memory cells to keep the information, what GRU can control is only the information inside the unit. The number and size of the hidden layer in the LSTM and GRU are set as 1 and 128 for the phase-resolved wave prediction.

2.3.2. MLP

As one of the most classical kinds of neural networks, MLP consists of three layers, i.e. the input layer, the middle hidden layer and the output layer. Each layer constitutes several neurons, while each connection between neurons has its own weight. The information flows

are unidirectionally transferred from the input layer to the output layer, passing through the hidden layers. Those perceptrons in the same layer share the same activation function, which is usually a sigmoid function for the hidden layer. The activation function for the output layer depends typically on the practical application, which can be a sigmoid or a linear function. The MLP used in the comparison study is a three-layer structure with a sigmoid activation function after the second layer. The output sizes of the first two layers of the MLP are 256 and 128, while the length of prediction steps determines the output size of the third layer.

2.3.3. CNN

CNN is originally employed for image pattern recognition with the ability to extract hierarchical features. Normally, CNN is constructed by four different layers: convolutional layer, non-linear activation layer, pooling layer and fully connected layer. With a set of kernels, convolutional layers convolve the input pixels, thereby generating the so-called feature map that summarizes the presence of detected features in the input. Then, the obtained feature map is activated by the element-wise non-linear activation layers. Next, pooling layers aggregate adjacent pixels based on the max or mean operation, which is not used in our wave prediction task. Finally, each node in the previous layer is directly connected to every node in the next layer by the fully connected layer. For comparison, the structure of CNN is designed the same as the CNN-branch (i.e. the CBR1, CBR2, CBR3, Conv and FCLayer2 in Fig. 3 with the detailed setting in Table 3) of the proposed DBNet.

2.3.4. DBNet

Obviously, both linear and non-linear relationships exist between the input historical wave information and output future wave elevation. Thus, for phase-resolved forecasting of 3D waves, a novel Dual-Branch Network is proposed where an extra MLP-based branch is designed to be parallel with a CNN-based branch for enhancing linear features and long-range dependencies. The structure of the proposed DBNet can be seen in Fig. 3.

The MLP-based branch is a relatively simple structure constructed with only a single fully connected layer without any activation function, i.e. FCLayer1 in Fig. 3. Without the activation function, the MLP is a linear regression model which can only learn linear relationships in the data. Meanwhile, as all input points are directly and fully connected by the MLP layer, the long-range dependencies between the input can be then captured. On the other hand, for the CNN-based branch, three convolutional layers with the Batch Normalization (BN) operation and the Rectified Linear Unit (ReLU) activation function, i.e. CBR1, CBR2 and CBR3, are stacked. With the ReLU, the non-linearity property can be introduced to the CNN-based branch. Finally, the output of the CBR3 is fed into a convolutional layer to reduce the number of feature map channels.

The features extracted by the MLP-based and CNN-based branches are added first and then fed into the final fully connected layer, i.e. FCLayer2, thereby generating the final future wave elevation sequence. The details of each component within the DBNet are provided in Table 3.

2.4. Model training

The data collected by the wave basin experiment are first re-sampled on a scale of 8, generating about 45,000 re-sampled points. Then, each re-sampled point represents 0.3 s in the real world. Thereafter, 40% of the re-sampled points (the first 18.0 min of each wave condition) are selected as the training set, 10% (18.0–22.5 min of each wave condition) for validation and 50% (the last 22.5 min of each wave condition) for testing. For training the machine learning models, the Mean Squared Error (MSE) is selected as the loss function:

$$\mathcal{L}(\mathcal{U}_{T+1:T+n}^4, \hat{\mathcal{U}}_{T+1:T+n}^4) = \frac{1}{n} \sum_{i=T+1}^{T+n} (u_i^4 - \hat{u}_i^4)^2 \quad (4)$$

By minimizing $\mathcal{L}(\cdot)$, the model is driven to approximate the real measured wave elevation as closely as possible.

2.5. Evaluation metrics

The performance of the ML-based models is evaluated by Mean Absolute Error (MAE) to measure the mean absolute difference and Root Mean Squared Error (RMSE) to reflect the square root of the average squared difference:

$$MAE = \frac{1}{N} \sum_{i=1}^N |\mathcal{U}_F - \hat{\mathcal{U}}_F| \quad (5)$$

$$RMSE = \sqrt{\frac{1}{N} \sum_{i=1}^N (\mathcal{U}_F - \hat{\mathcal{U}}_F)^2} \quad (6)$$

where N is the whole number of predictions in the test set, while \mathcal{U}_F and $\hat{\mathcal{U}}_F$ represent the measured and predicted future wave elevations respectively. The metrics are then normalized by the corresponding significant height to observe the relative errors:

$$MAE\% = \frac{MAE}{H_s} \times 100\% \quad (7)$$

$$RMSE\% = \frac{RMSE}{H_s} \times 100\% \quad (8)$$

3. Results and discussions

To comprehensively analyze the phase-resolved forecasting of 3D waves, two prediction scenarios, i.e. wave forecasting using upstream information and local information, are designed. In the first scenario, the performance of all five methods is thoroughly compared. Then, the significance of the directional information is verified by the comparative studies. Finally, the impacts of the different lengths of input and output time horizons are investigated. In the second scenario, using the local wave information as the input, all five methods are compared first and then the errors with different output future time horizons are explored.

3.1. Wave forecasting using upstream information

In this part, wave forecasting using upstream information is investigated. Specifically, the input of models is set as the historical upstream wave information measured by the gauge array, i.e. WG2, WG5, WG6, WG7 and WG8, while the target output is the future wave elevation measured by WG4.

3.1.1. Performance of different methods

Five machine learning methods are trained by the data of all nine wave conditions under three sea states. That is to say, each model is designed to learn mapping relationships between input and output for all nine wave conditions simultaneously instead of training three different models for three sea states. In these studies, the length of input points is set as 300 (90 s in full scale) and 85 for output (25.5 s in full scale).

As shown in Table 4, all ML-based models can perform relatively well, especially considering the unavoidable noises during the wave basin experiments. Although the MAE and RMSE have considerable disparity for different wave conditions, the relative errors, i.e. MAE% and RMSE% normalized by the significant height, maintain the same level, demonstrating that the normalized prediction errors are better metrics for overall performance.

The prediction errors of two RNN models, i.e. GRU and LSTM, are larger than other methods, whose average RMSE% are about 12.1%. The reason is that it is still an extremely challenging task for RNNs to learn dependencies between distant positions, especially for long input sequences, albeit LSTM and GRU have been specifically optimized to resolve the short-term memory problem. The results of MLP and CNN are slightly better than RNN models and have similar error levels, which are about 11.9% and 12.0% measured by RMSE%.

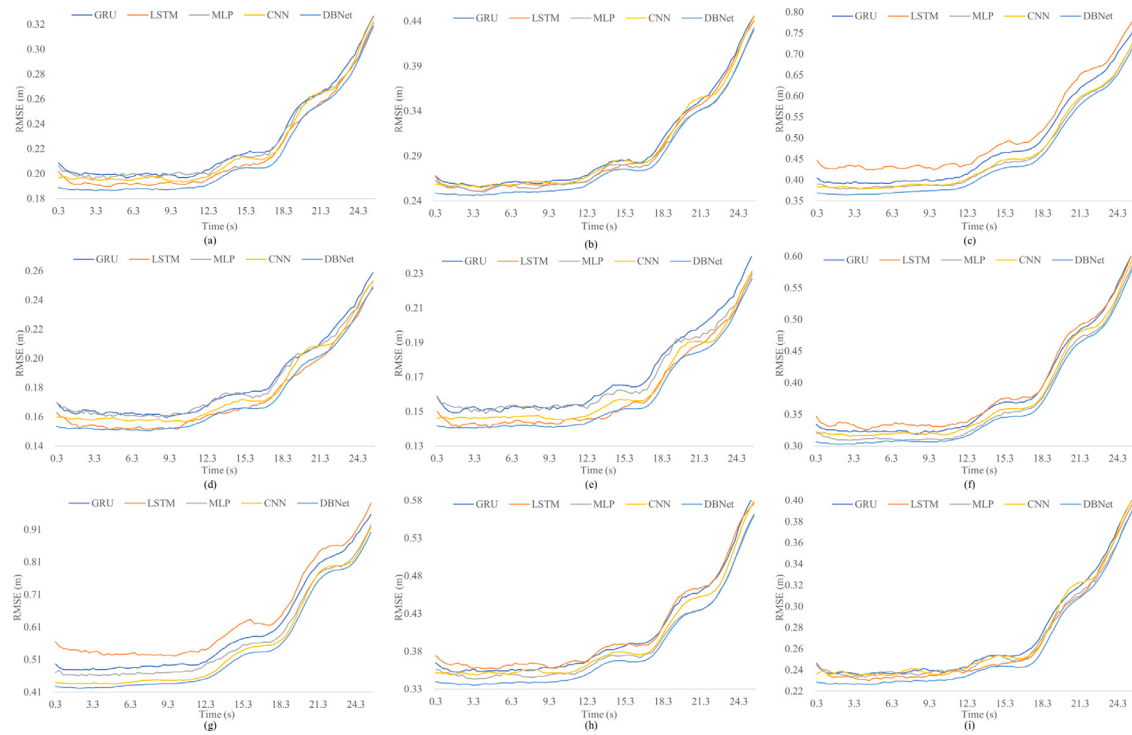


Fig. 4. The error distributions of ML-based methods over the whole prediction time domain using upstream historical wave information measured by WG2, WG5, WG6, WG7 and WG8, where the error for each time step is averaged over all the experimental wave data in the test set. (a)–(i) represent the nine wave conditions.

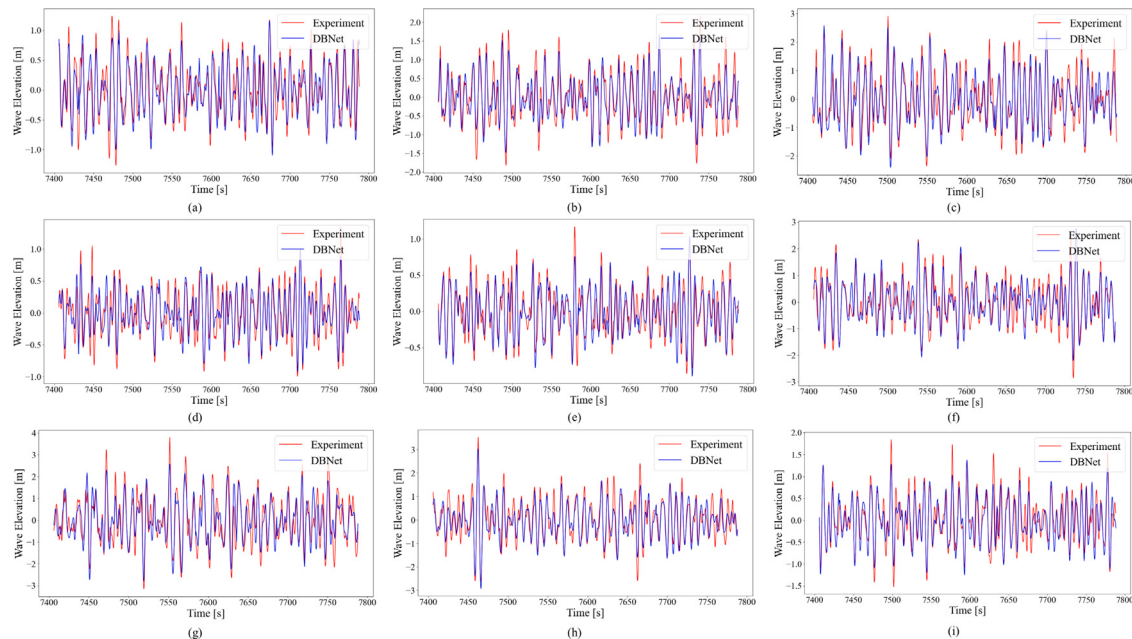


Fig. 5. The wave elevations measured in experiments (red) and the prediction results by DBNet (blue) during the 7400 s to 7800 s, where the inputs are the upstream historical wave information measured by WG2, WG5, WG6, WG7 and WG8. (a)–(i) represent the nine wave conditions.

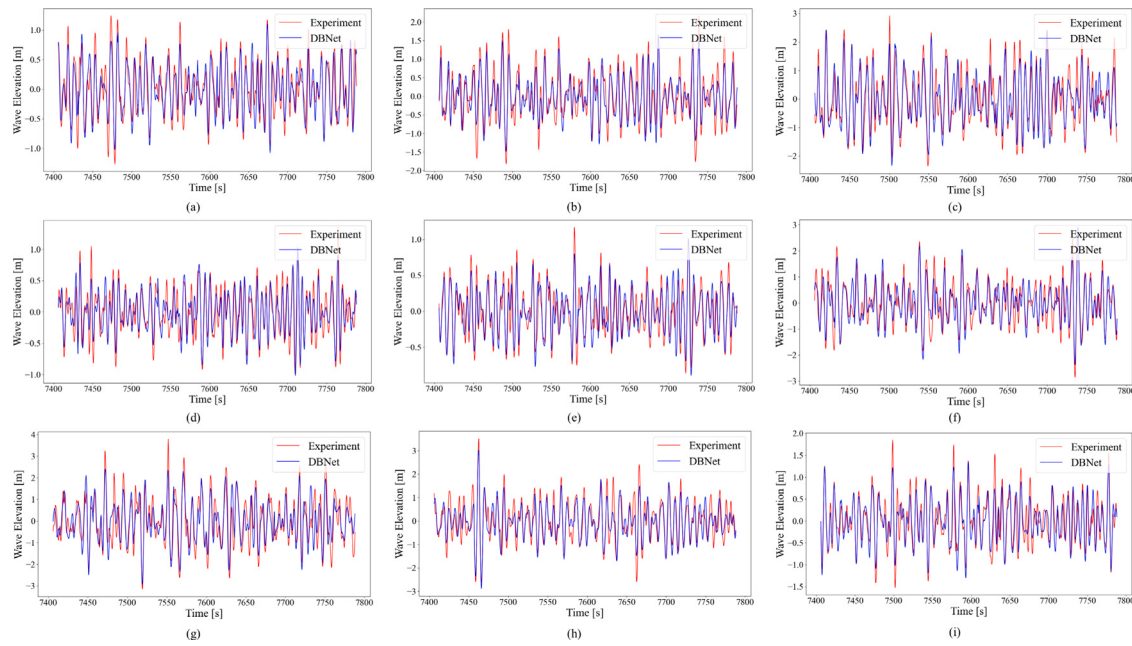


Fig. 6. The wave elevations measured in experiments (red) and the prediction results by DBNet (blue) during the 7400 s to 7800 s, where the inputs are the upstream historical wave information measured by WG2, WG7 and WG8. (a)–(i) represent the nine wave conditions.

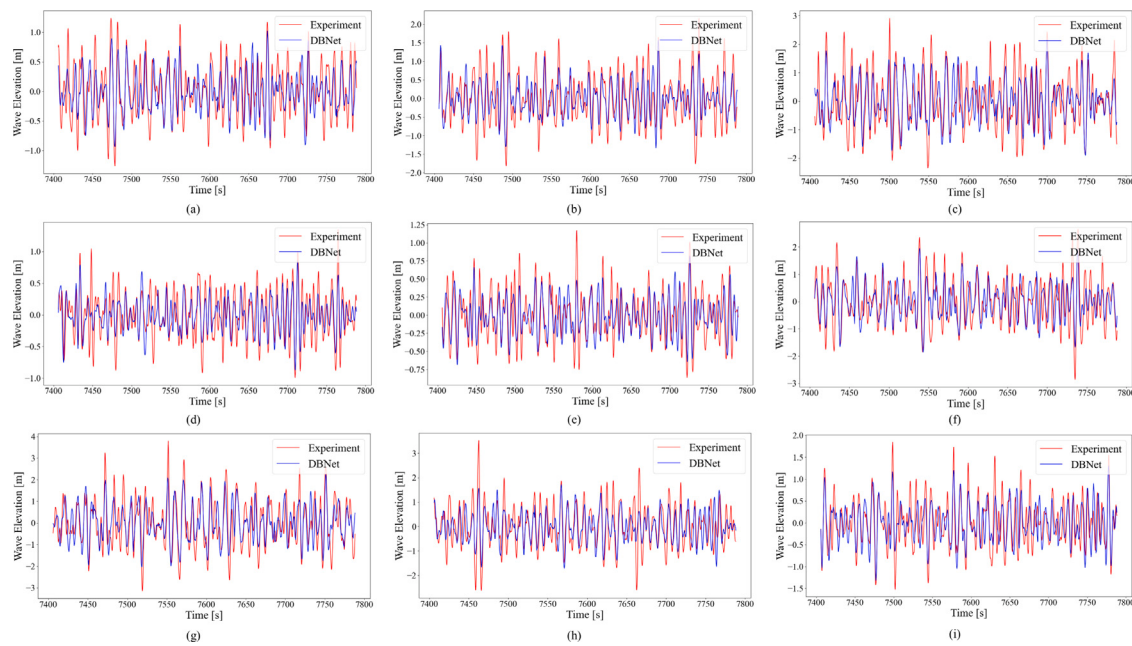


Fig. 7. The wave elevations measured in experiments (red) and the prediction results by DBNet (blue) during the 7400 s to 7800 s, where the inputs are the upstream historical wave information measured by WG2. (a)–(i) represent the nine wave conditions.

Table 4

The prediction errors measured by MAE (m), RMSE (m), MAE% and RMSE% for all methods under nine wave conditions using upstream wave information. Each method is trained, validated and tested ten times and then the means and standard deviations are reported. Please notice the MAE and RMSE are transformed to the full scale.

Con.	Method	MAE	RMSE	MAE%	RMSE%
1	GRU	0.17528 ± 0.00146	0.22353 ± 0.00168	9.348 ± 0.078	11.992 ± 0.090
	LSTM	0.16986 ± 0.00166	0.21681 ± 0.00210	9.059 ± 0.089	11.563 ± 0.112
	MLP	0.17756 ± 0.00079	0.22590 ± 0.00094	9.470 ± 0.042	12.048 ± 0.050
	CNN	0.17587 ± 0.00146	0.22427 ± 0.00172	9.380 ± 0.078	11.961 ± 0.092
	DBNet	0.16982 ± 0.00057	0.21704 ± 0.00068	9.057 ± 0.030	11.576 ± 0.036
2	GRU	0.23358 ± 0.00117	0.29686 ± 0.00162	9.160 ± 0.046	11.642 ± 0.063
	LSTM	0.23086 ± 0.00172	0.29357 ± 0.00228	9.053 ± 0.068	11.513 ± 0.090
	MLP	0.23035 ± 0.00064	0.29246 ± 0.00082	9.033 ± 0.025	11.469 ± 0.032
	CNN	0.23611 ± 0.00190	0.29936 ± 0.00225	9.259 ± 0.075	11.740 ± 0.088
	DBNet	0.22900 ± 0.00063	0.29079 ± 0.00081	8.980 ± 0.025	11.404 ± 0.032
3	GRU	0.37291 ± 0.00264	0.47972 ± 0.00337	9.323 ± 0.066	11.993 ± 0.084
	LSTM	0.38649 ± 0.00574	0.49763 ± 0.00716	9.662 ± 0.143	12.441 ± 0.179
	MLP	0.36157 ± 0.00132	0.46534 ± 0.00157	9.039 ± 0.033	11.633 ± 0.039
	CNN	0.36894 ± 0.00305	0.47399 ± 0.00369	9.223 ± 0.076	11.850 ± 0.092
	DBNet	0.35724 ± 0.00116	0.46019 ± 0.00141	8.931 ± 0.029	11.505 ± 0.035
4	GRU	0.14331 ± 0.00133	0.18155 ± 0.00169	10.237 ± 0.095	12.968 ± 0.120
	LSTM	0.13547 ± 0.00177	0.17171 ± 0.00230	9.676 ± 0.126	12.265 ± 0.164
	MLP	0.14465 ± 0.00070	0.18350 ± 0.00089	10.322 ± 0.050	13.107 ± 0.064
	CNN	0.14141 ± 0.00115	0.17914 ± 0.00140	10.100 ± 0.082	12.796 ± 0.100
	DBNet	0.13731 ± 0.00037	0.17408 ± 0.00047	9.808 ± 0.027	12.435 ± 0.033
5	GRU	0.13460 ± 0.00112	0.17076 ± 0.00128	10.159 ± 0.085	12.888 ± 0.096
	LSTM	0.12573 ± 0.00143	0.15936 ± 0.00182	9.489 ± 0.108	12.027 ± 0.138
	MLP	0.13581 ± 0.00070	0.17061 ± 0.00086	10.250 ± 0.053	12.876 ± 0.065
	CNN	0.12979 ± 0.00082	0.16440 ± 0.00098	9.795 ± 0.062	12.408 ± 0.074
	DBNet	0.12606 ± 0.00034	0.15976 ± 0.00043	9.514 ± 0.025	12.057 ± 0.032
6	GRU	0.30010 ± 0.00146	0.38391 ± 0.00201	8.892 ± 0.043	11.375 ± 0.059
	LSTM	0.30250 ± 0.00277	0.38762 ± 0.00342	8.963 ± 0.082	11.485 ± 0.101
	MLP	0.29169 ± 0.00081	0.37382 ± 0.00104	8.643 ± 0.024	11.076 ± 0.031
	CNN	0.30098 ± 0.00268	0.38554 ± 0.00312	8.918 ± 0.080	11.423 ± 0.093
	DBNet	0.29096 ± 0.00098	0.37358 ± 0.00119	8.621 ± 0.029	11.069 ± 0.035
7	GRU	0.46248 ± 0.00296	0.60028 ± 0.00428	9.685 ± 0.062	12.571 ± 0.090
	LSTM	0.48255 ± 0.00936	0.62557 ± 0.01156	10.106 ± 0.196	13.101 ± 0.242
	MLP	0.44957 ± 0.00193	0.58447 ± 0.00256	9.415 ± 0.041	12.240 ± 0.054
	CNN	0.44456 ± 0.00324	0.57721 ± 0.00383	9.310 ± 0.068	12.088 ± 0.080
	DBNet	0.43487 ± 0.00126	0.56505 ± 0.00151	9.107 ± 0.026	11.833 ± 0.032
8	GRU	0.31521 ± 0.00121	0.39941 ± 0.00162	9.552 ± 0.037	12.103 ± 0.049
	LSTM	0.31813 ± 0.00171	0.40338 ± 0.00228	9.640 ± 0.052	12.224 ± 0.069
	MLP	0.30688 ± 0.00071	0.38868 ± 0.00096	9.299 ± 0.022	11.778 ± 0.029
	CNN	0.31537 ± 0.00348	0.39990 ± 0.00447	9.557 ± 0.105	12.118 ± 0.135
	DBNet	0.30607 ± 0.00088	0.38793 ± 0.00114	9.275 ± 0.027	11.755 ± 0.035
9	GRU	0.21181 ± 0.00135	0.26933 ± 0.00149	9.209 ± 0.059	11.710 ± 0.065
	LSTM	0.20713 ± 0.00148	0.26357 ± 0.00195	9.006 ± 0.064	11.460 ± 0.085
	MLP	0.21177 ± 0.00072	0.26821 ± 0.00091	9.207 ± 0.031	11.662 ± 0.040
	CNN	0.21464 ± 0.00199	0.27282 ± 0.00237	9.332 ± 0.086	11.862 ± 0.103
	DBNet	0.20760 ± 0.00066	0.26401 ± 0.00080	9.026 ± 0.029	11.479 ± 0.035
Avg.	GRU	0.26103 ± 0.00163	0.33393 ± 0.00212	9.435 ± 0.059	12.070 ± 0.076
	LSTM	0.26208 ± 0.00307	0.33547 ± 0.00387	9.473 ± 0.111	12.125 ± 0.140
	MLP	0.25665 ± 0.00093	0.32811 ± 0.00117	9.277 ± 0.034	11.859 ± 0.042
	CNN	0.25863 ± 0.00220	0.33074 ± 0.00265	9.348 ± 0.080	11.954 ± 0.096
	DBNet	0.25099 ± 0.00076	0.32138 ± 0.00094	9.072 ± 0.027	11.616 ± 0.034

For the proposed DBNet, as the parallel structure combines the advantages of both CNN and MLP, the errors measured by MAE and RMSE are the lowest for all nine wave conditions among five ML-based methods. As for the average error, the performance of the DBNet is about 0.2% better than the sub-optimal MLP in MAE% and RMSE%. Most importantly, the developed DBNet is a computational-friendly model. It takes only 2772 s to complete the whole training procedure on a standard desktop with a single Intel Core i7-7700 CPU and 32, 768 MB RAM, while the prediction for a 25.5 s time horizon only costs 0.865 s (including the whole data processing and model loading procedure) which obviously meets the real-time requirement. As what most active control systems require is about a 20 s future time horizon [20], a 25.5 s prediction is enough for the control-oriented wave elevation prediction, indicating the huge potential of the proposed DBNet for the model predictive control of WECs.

In Fig. 4, in order to visually identify the prediction accuracy of different ML-based wave prediction methods, the error distributions over the whole prediction time domain, i.e. 85 prediction points for 25.5 s in the real world, are investigated. The RMSE of the prediction results compared with the experimental values for five ML-based methods at different time horizons are calculated and visualized, where the RMSE for each time step is averaged over all the experimental wave data in the test set. As can be seen, the error distribution tendencies of all ML-based methods are quite similar for all nine wave conditions. Specifically, the errors are relatively low and stable for the first 12.0 s, which experience a gradual growth during 12.0 s to 17.4 s and then grow rapidly and finally reach the peak at 25.5 s where the error is about twice that of the initial stage. Such a tendency is related to the theoretically predictable zone, whose physically meaningful boundaries can be explained based on the linear theory of wave propagation. To be specific, in our case, the historical wave information is recorded by

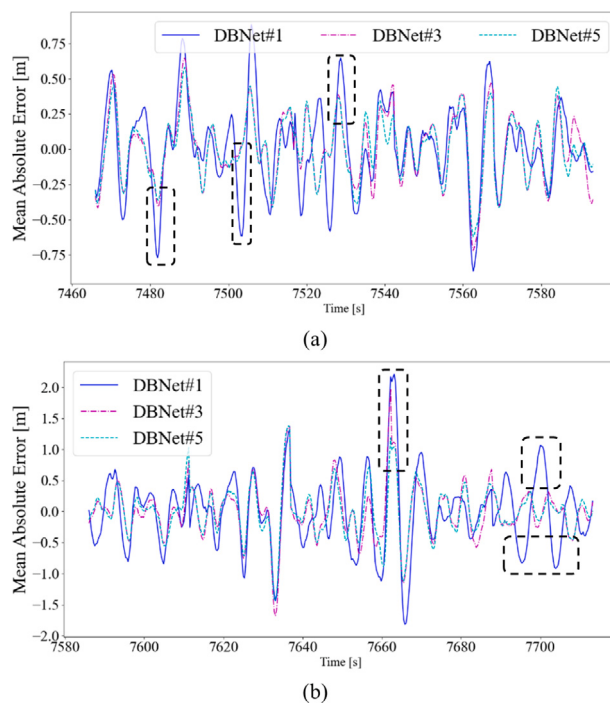


Fig. 8. The absolute errors of three types of input with different upstream gauges data. (a) wave condition 1 during 7460 s to 7600 s and (b) wave condition 8 during 7580 s to 7720 s, where DBNet#1, DBNet#3 and DBNet#5 represent the input from 1, 3 and 5 upstream gauges.

the upstream gauges (i.e. WG2, WG5, WG6, WG7 and WG8). Then, the beginning and the end of the theoretically predictable zone are moments when recorded wave components at the upstream gauges fully reach the downstream gauge (i.e. WG4) and those components initially leave the downstream gauge, respectively. In other words, the boundaries are determined respectively by the timings that the slowest wave passes the downstream gauge at the earliest time and the fastest wave passes the downstream gauge at the latest time. Thus, the increased errors in the last period beyond the predictable zone are reasonable and expected. More analyses about the theoretically predictable zone can refer to [17,45].

For all nine wave conditions, the proposed DBNet holds the lead in most of the prediction time horizons, demonstrating the advantage of the DBNet compared with other ML-based methods. Another superiority of the DBNet is the better prediction performance during the first 12.0 s, which is especially obvious for wave conditions 1–3 (Fig. 4(a)–(c)) and wave conditions 7–9 (Fig. 4(g)–(i)). In Fig. 5, we further illustrate the wave elevations measured in the experiments and the predicted results by the proposed DBNet during the 7400 s to 7800 s for nine wave conditions. As can be seen, the predicted results of the DBNet show a high agreement with the experimental data under all nine wave conditions. Taking wave condition 3 (Fig. 5(c)) as an example, the wave elevation experiences a dramatic surge at around 7700 s which increases from about -1.5 m to almost 2.5 m directly. The proposed DBNet successfully tracks this striking change with quite a high accuracy.

3.1.2. The significance of the directional information

The comparative studies are conducted in this section to investigate the significance of the directional information in predictions of 3D waves. Specifically, the directional information is implicit within the data measured by the pentagonal gauge array (WG2, WG5, WG6, WG7 and WG8). Thus, two additional studies are conducted based on the proposed DBNet: the input upstream wave information for the former is measured by WG2, WG7 and WG8, while the latter is only WG2.



Fig. 9. The prediction errors measured by MAE and RMSE using upstream wave information for different lengths of the (a) output time horizon and the (b) input time horizon.

The quantitative comparison between three input scenarios can be seen in Table 5. Apparently, the wave data measured by three gauges contain less directional information than those of five gauges. Thus, the errors of the DBNet with input measured by three gauges increase marginally for all wave conditions. As the directional information can be still extracted from three upstream gauges, the average MAE% and RMSE% merely witness a slight increase from 9.1% to 9.6% and 11.6% to 12.3%, respectively. In sharp contrast, when the input becomes the data only from a single gauge, i.e. without any directional information, the errors obviously surge to a high level, which increases by more than 4.0% in MAE% and 5.0% in RMSE%.

The prediction results of those two scenarios can be seen in Figs. 6 and 7. With three upstream wave gauges, the DBNet demonstrates a satisfactory performance which holds a similar accuracy compared with the prediction with five upstream wave gauges. However, when only a single upstream gauge is available, the prediction errors dramatically rise to a very high level, especially for those scenarios with tremendous changes. For example, the wave emerges a violent fluctuation at about 7460 s in Fig. 7(h). Although the fluctuation trend is correctly captured and predicted by the model, the prediction accuracy is far from satisfactory which is more than 1.0 m (30% normalized by the significant height) measured by MAE. Two cases of absolute errors with three types of input are visually illustrated in Fig. 8, where black dashed rectangles mark the typical discrepancies between three circumstances. Clearly, the error level of only one gauge's input is significantly higher than the other two scenarios. By comparison, the error distributions between the circumstances with three and five gauges' inputs are quite similar along the time span, indicating that the directional information is indeed necessary for the model to extract and reconstruct the features of 3D waves. From the above studies and comparisons, we can conclude that directional information plays an important role in the phase-resolved forecasting of 3D waves.

Table 5

The prediction errors measured by MAE (m), RMSE (m), MAE% and RMSE% using different upstream gauges under nine wave conditions. Each method is trained, validated and tested ten times and then the means are reported. Please notice the MAE and RMSE are transformed to the full scale.

Con.	Gauges	MAE	RMSE	MAE%	RMSE%
1	1	0.24981	0.31430	13.323	16.763
	3	0.17971	0.23083	9.585	12.311
	5	0.16982	0.21704	9.057	11.576
2	1	0.34404	0.43165	13.492	16.927
	3	0.24139	0.30837	9.466	12.093
	5	0.22900	0.29079	8.980	11.404
3	1	0.50390	0.63715	12.597	15.929
	3	0.37912	0.49164	9.478	12.291
	5	0.35724	0.46019	8.931	11.505
4	1	0.20476	0.25627	14.626	18.305
	3	0.14460	0.18351	10.329	13.108
	5	0.13731	0.17408	9.808	12.435
5	1	0.18546	0.23155	13.997	17.476
	3	0.13273	0.16899	10.017	12.754
	5	0.12606	0.15976	9.514	12.057
6	1	0.43366	0.54544	12.849	16.161
	3	0.30599	0.39555	9.066	11.720
	5	0.29096	0.37358	8.621	11.069
7	1	0.59221	0.75581	12.402	15.828
	3	0.46057	0.60673	9.645	12.706
	5	0.43487	0.56505	9.107	11.833
8	1	0.46168	0.58463	13.990	17.716
	3	0.31845	0.40610	9.650	12.306
	5	0.30607	0.38793	9.275	11.755
9	1	0.31477	0.39539	13.686	17.191
	3	0.21823	0.27934	9.488	12.145
	5	0.20760	0.26401	9.026	11.479
Avg.	1	0.36559	0.46136	13.214	16.676
	3	0.26453	0.34123	9.561	12.334
	5	0.25099	0.32138	9.072	11.616

3.1.3. The length of input and output time horizon

Intuitively, the difficulty of phase-resolved wave forecasting will be positively associated with the length of the output but negatively correlated with the length of the input. In this part, the above hypothesis is explored by quantitative tests. Five output time horizons, i.e. 22.5 s, 24.0 s, 25.5 s, 27.0 s and 28.5 s and five input time horizons, i.e. 130 s, 110 s, 90 s, 70 s and 50 s are compared using the proposed DBNet.

The prediction errors of these settings are reported in Fig. 9. As can be seen, the errors indeed increase with the extended length of the prediction time horizon, especially for those longer than 25.5 s. For the input sequence, the impact of the length is not very obvious, especially for those longer than 90 s.

3.2. Wave forecasting using local information

In this part, wave forecasting using local information is investigated. To be specific, the input of models is set as the historical local wave information measured by WG4 itself, while the target output is the future wave elevation measured by WG4.

3.2.1. Performance of different methods

Apparently, as the input only contains local wave data without either directional information or upstream historical wave elevation, the predictable time horizon is expected to be much shorter than the scenario with the upstream wave data. Thus, a small prediction time horizon (4.5 s) is selected in this condition, while the input historical time horizon is still 90 s.

As shown in Table 6, even though all ML-based methods have a decent performance, the errors of GRU and LSTM are still more considerable than others due to the long input sequences. Since the

output is a relatively short sequence, the gaps between MLP, CNN and DBNet are very small, but the proposed DBNet still holds a slim advantage.

The measured wave elevation and predicted results by the proposed DBNet during the 7400 s to 7800 s are shown in Fig. 10. As illustrated, the predictions most often match with the measured wave elevation (which is used as the reference value). For example, at about 7475 s in Fig. 10(a), the wave considerably fluctuates from around -1.3 m to 1.3 m three times, while the proposed DBNet nicely predicts such striking changes with very small errors. Meanwhile, some differences exist between peaks in the experiment results and DBNet predictions. The first reason is that the local wave measured by the WG4 itself does not contain any direction information. As shown in Section 3.1.2, the direction information is actually essential for the phase-resolved prediction of 3D waves. The second factor which undermines prediction accuracy is the existence of inevitable measurement errors.

3.2.2. The length of output time horizon

This part investigates wave forecasting using local information for different lengths of future time horizons. Specifically, taking the same length (90 s) of historical local wave information measured by WG4 as the input, the prediction errors for different output time horizons including 4.5 s, 5.1 s and 6.0 s are explored.

As shown in Fig. 11, the errors obviously enlarge with the increase of the prediction time horizons. For example, when predicting future 6.0 s wave elevation, the RMSE increases more than 20% compared with the 4.5 s time horizon, indicating the limited predictable future time horizon using local wave information.

3.3. Ablation study about the hyper-parameters

In this part, the ablation study about the hyper-parameters of different machine learning methods used in our work is conducted. For the ablation study, the input is set as the 90 s historical wave information measured by the upstream gauges and the output is the 25.5 s future downstream wave elevation. All methods are trained and tested ten times and the average MAE and RMSE are reported in Fig. 12. To investigate the effect of the number of convolutional layers, we add a CBR and delete a CBR in the DBNet and the CNN, respectively. As seen in Fig. 12, either adding a CBR (DBNet1 and CNN1) or deleting a CBR (DBNet2 and CNN2) can lead to a marginal decrease in accuracy. For MLP, the output sizes of the first two layers are set as (128, 64) to construct MLP1 and (512, 256) to build MLP2. However, both of those two modifications would weaken the performance. As to LSTM and GRU, the number and size of the hidden layer for LSTM1 and GRU1 are set as 1 and 256, while LSTM2 and GRU2 are 2 and 128. The results demonstrate that the increase in the size of the hidden layer would slightly increase errors, while errors would obviously rise with the increase in the number of hidden layers. Based on this ablation study, the final hyper-parameters used in this work are obtained which are reported in Section 2.3.

3.4. Discussion

It is worth mentioning that the phase-resolved forecasting of 3D waves based on local wave information only requires the local wave measurement which is usually directly available, while the prediction based on the upstream wave information, as investigated in Section 3.1, requires additional upstream wave measurement. However, the local wave data can only meet the very short-term wave prediction requirement within 5 s which is far from the standard of control-oriented wave forecasting (at least 20 s future wave elevation [20]). By contrast, although the measurement process is more complicated and expensive (at least three gauges installed on the upstream), the upstream information can be used for control-oriented wave forecasting. Thus, these two kinds of formulations have their corresponding advantages

Table 6

The prediction errors measured by MAE (m), RMSE (m), MAE% and RMSE% for all methods under nine wave conditions using local wave information. Each method is trained, validated and tested ten times and then the means and standard deviations are reported. Note that the MAE and RMSE are transformed to the full scale.

Con.	Methods	MAE	RMSE	MAE%	RMSE%
1	GRU	0.16417 ± 0.00049	0.22038 ± 0.00061	8.755 ± 0.026	11.754 ± 0.033
	LSTM	0.15601 ± 0.00134	0.21236 ± 0.00197	8.320 ± 0.071	11.326 ± 0.105
	MLP	0.15957 ± 0.00072	0.21562 ± 0.00111	8.510 ± 0.039	11.500 ± 0.059
	CNN	0.15755 ± 0.00282	0.21580 ± 0.00318	8.403 ± 0.150	11.510 ± 0.170
	DBNet	0.15673 ± 0.00226	0.21484 ± 0.00263	8.359 ± 0.120	11.458 ± 0.140
2	GRU	0.21852 ± 0.00151	0.29513 ± 0.00203	8.569 ± 0.059	11.574 ± 0.080
	LSTM	0.21212 ± 0.00226	0.28839 ± 0.00279	8.319 ± 0.089	11.309 ± 0.110
	MLP	0.20889 ± 0.00111	0.28459 ± 0.00145	8.192 ± 0.043	11.160 ± 0.057
	CNN	0.21098 ± 0.00380	0.28875 ± 0.00421	8.274 ± 0.149	11.324 ± 0.165
	DBNet	0.20985 ± 0.00298	0.28753 ± 0.00345	8.230 ± 0.117	11.276 ± 0.135
3	GRU	0.36341 ± 0.00421	0.48700 ± 0.00547	9.085 ± 0.105	12.175 ± 0.137
	LSTM	0.36377 ± 0.00573	0.48608 ± 0.00674	9.094 ± 0.143	12.152 ± 0.168
	MLP	0.34212 ± 0.00181	0.46200 ± 0.00191	8.553 ± 0.045	11.550 ± 0.048
	CNN	0.33802 ± 0.00563	0.45751 ± 0.00542	8.450 ± 0.141	11.438 ± 0.135
	DBNet	0.33643 ± 0.00412	0.45566 ± 0.00429	8.411 ± 0.103	11.392 ± 0.107
4	GRU	0.12599 ± 0.00076	0.17020 ± 0.00115	8.999 ± 0.054	12.157 ± 0.082
	LSTM	0.11840 ± 0.00191	0.16333 ± 0.00250	8.457 ± 0.136	11.666 ± 0.179
	MLP	0.12761 ± 0.00092	0.17365 ± 0.00145	9.115 ± 0.066	12.404 ± 0.104
	CNN	0.12533 ± 0.00246	0.17302 ± 0.00282	8.952 ± 0.176	12.359 ± 0.201
	DBNet	0.12473 ± 0.00213	0.17237 ± 0.00251	8.909 ± 0.152	12.312 ± 0.179
5	GRU	0.12339 ± 0.00052	0.16616 ± 0.00092	9.313 ± 0.039	12.540 ± 0.070
	LSTM	0.11541 ± 0.00210	0.15833 ± 0.00267	8.710 ± 0.158	11.950 ± 0.201
	MLP	0.12472 ± 0.00092	0.16894 ± 0.00136	9.413 ± 0.069	12.750 ± 0.103
	CNN	0.12085 ± 0.00248	0.16638 ± 0.00276	9.121 ± 0.187	12.557 ± 0.209
	DBNet	0.12040 ± 0.00211	0.16587 ± 0.00245	9.087 ± 0.159	12.518 ± 0.185
6	GRU	0.29478 ± 0.00316	0.39612 ± 0.00384	8.734 ± 0.094	11.737 ± 0.114
	LSTM	0.29204 ± 0.00338	0.39352 ± 0.00392	8.653 ± 0.100	11.660 ± 0.116
	MLP	0.28053 ± 0.00145	0.38047 ± 0.00161	8.312 ± 0.043	11.273 ± 0.048
	CNN	0.27810 ± 0.00495	0.37777 ± 0.00507	8.240 ± 0.147	11.193 ± 0.150
	DBNet	0.27683 ± 0.00374	0.37640 ± 0.00403	8.202 ± 0.111	11.153 ± 0.119
7	GRU	0.45898 ± 0.00707	0.60425 ± 0.00891	9.612 ± 0.148	12.654 ± 0.187
	LSTM	0.47510 ± 0.00952	0.62322 ± 0.01080	9.950 ± 0.199	13.052 ± 0.226
	MLP	0.43218 ± 0.00255	0.57684 ± 0.00299	9.051 ± 0.053	12.081 ± 0.063
	CNN	0.42723 ± 0.00658	0.57535 ± 0.00552	8.947 ± 0.138	12.049 ± 0.116
	DBNet	0.42557 ± 0.00442	0.57300 ± 0.00404	8.913 ± 0.093	12.000 ± 0.085
8	GRU	0.29070 ± 0.00245	0.39550 ± 0.00357	8.809 ± 0.074	11.985 ± 0.108
	LSTM	0.28752 ± 0.00329	0.39208 ± 0.00407	8.713 ± 0.100	11.881 ± 0.123
	MLP	0.27744 ± 0.00151	0.38202 ± 0.00192	8.407 ± 0.046	11.576 ± 0.058
	CNN	0.27993 ± 0.00517	0.38556 ± 0.00579	8.483 ± 0.157	11.684 ± 0.176
	DBNet	0.27899 ± 0.00348	0.38477 ± 0.00419	8.454 ± 0.105	11.660 ± 0.127
9	GRU	0.19582 ± 0.00074	0.26490 ± 0.00114	8.514 ± 0.032	11.517 ± 0.050
	LSTM	0.18822 ± 0.00166	0.25686 ± 0.00222	8.184 ± 0.072	11.168 ± 0.096
	MLP	0.18857 ± 0.00097	0.25661 ± 0.00133	8.199 ± 0.042	11.157 ± 0.058
	CNN	0.19031 ± 0.00327	0.26062 ± 0.00365	8.274 ± 0.142	11.331 ± 0.159
	DBNet	0.18940 ± 0.00256	0.25950 ± 0.00302	8.235 ± 0.111	11.283 ± 0.131
Avg.	GRU	0.24842 ± 0.00232	0.33329 ± 0.00307	8.979 ± 0.084	12.047 ± 0.111
	LSTM	0.24540 ± 0.00347	0.33046 ± 0.00419	8.870 ± 0.125	11.944 ± 0.151
	MLP	0.23796 ± 0.00133	0.32231 ± 0.00168	8.601 ± 0.048	11.650 ± 0.061
	CNN	0.23648 ± 0.00413	0.32231 ± 0.00427	8.547 ± 0.149	11.650 ± 0.154
	DBNet	0.23544 ± 0.00309	0.32110 ± 0.00340	8.510 ± 0.112	11.606 ± 0.123

and disadvantages. Therefore, they will target different application scenarios according to the specific needs. Based on the experiments conducted in this paper, the main findings are summarized as:

- (1) The ML methods can achieve the real-time deterministic forecasting of 3D waves (with a time horizon of more than 20 s) based on the historical upstream wave information measured by the gauge array. The forecasting time horizon is sufficient to enable preview-based control of WECs.
- (2) The study shows that the directional wave information captured by the upstream wave gauge array is necessary for achieving accurate wave forecasting. Also, the errors of phase-resolved wave forecasting are positively associated with the length of the output and negatively correlated with the length of the input.

(3) The results also demonstrate that with the local historical information (which can be obtained more easily compared with the directional upstream information) as the input, the ML methods can achieve very short-term wave forecasting (i.e. 4.5 s) accurately.

4. Conclusions

To the best of our knowledge, this work investigated, for the first time, the phase-resolved real-time prediction of 3D waves based on ML and wave tank experiments. Two major barriers in phase-resolved wave prediction, i.e. the generalization of the model to diverse sea states and the deterministic prediction of 3D waves, were both resolved. Specifically, the experimental results demonstrated that the set of ML models

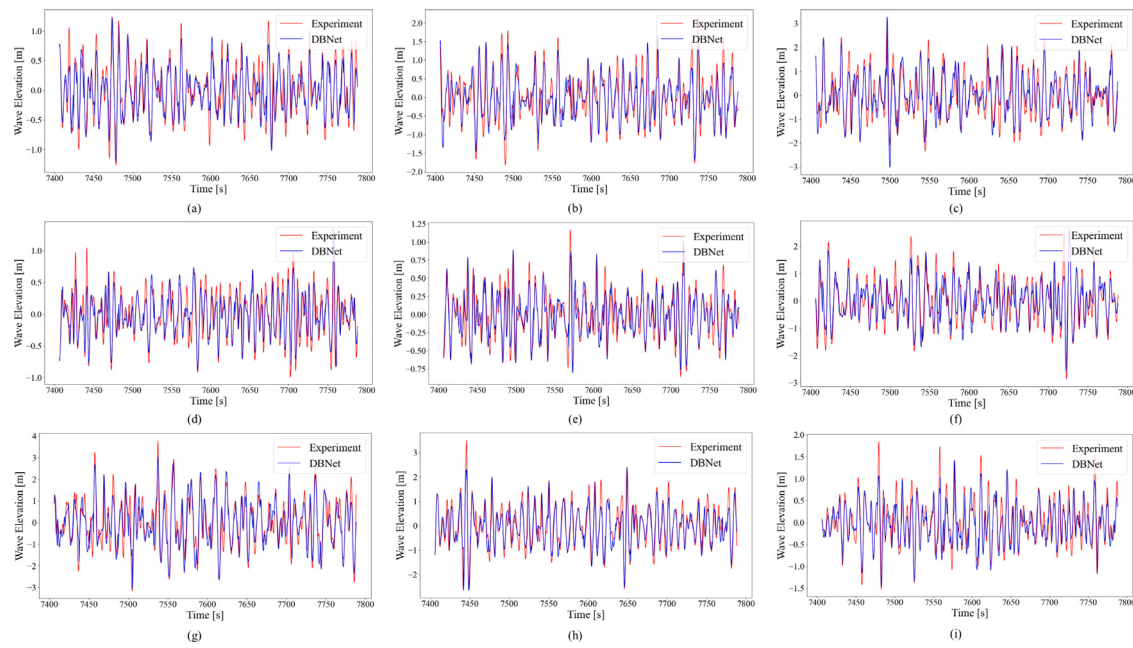


Fig. 10. The wave elevations measured in experiments (red) and the prediction results by DBNet (blue) during the 7400 s to 7800 s, where the inputs are the local historical wave information measured by WG4. (a)–(i) represent the nine wave conditions.

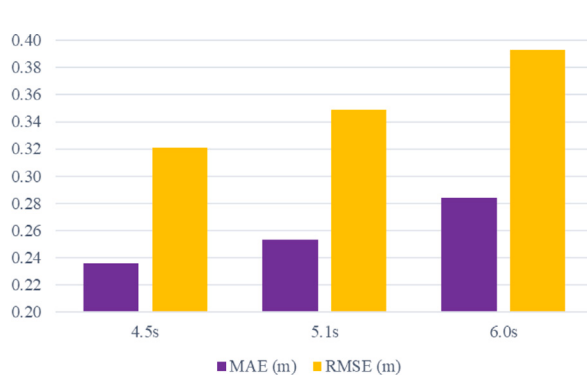


Fig. 11. The prediction errors measured by MAE and RMSE using local wave information for different lengths of the output time horizon.

developed in this paper was effective for different wave conditions and sea states without retraining multiple times. In particular, the proposed DBNet showed better performance than other ML methods.

The preview-based hydrodynamic control is a very important and effective strategy to improve the power generation of WECs [7] significantly. However, as a non-causal optimal control problem, forecasting for future wave elevations with at least a 20 s time horizon is normally required for those WEC controllers [20]. Thus, the machine learning model proposed in this work, which can achieve the control-oriented phase-resolved prediction of 3D waves for multiple sea states in real-time, is greatly useful to enable the MPC approaches to enhance the energy conversion efficiency of WECs. Our future works may involve the investigation of more sea states, the validation of the model to full-scale wave data measured in real-world ocean sites, and the application of the proposed model for WEC controller optimization.

CRediT authorship contribution statement

Rui Li: Conceptualization, Data curation, Formal analysis, Investigation, Methodology, Project administration, Software, Validation, Visualization, Writing – original draft. **Jincheng Zhang:** Conceptualization, Data curation, Formal analysis, Investigation, Methodology, Project administration, Software, Visualization, Writing – review & editing. **Xiaowei Zhao:** Conceptualization, Formal analysis, Funding acquisition, Investigation, Methodology, Project administration, Resources, Supervision, Writing – review & editing. **Daming Wang:** Data curation, Investigation, Project administration, Writing – review & editing. **Martyn Hann:** Resources, Supervision, Writing – review & editing. **Deborah Greaves:** Funding acquisition, Investigation, Project administration, Resources, Supervision, Writing – review & editing.

Declaration of competing interest

The authors declare that they have no known competing financial interests or personal relationships that could have appeared to influence the work reported in this paper.

Data availability

Data will be made available on request.

Acknowledgments

This work has received funding from the UK Engineering and Physical Sciences Research Council (grant number: EP/S000747/1). The authors acknowledge the Scientific Computing Research Technology Platform (SCRTP) at the University of Warwick for providing High-Performance Computing resources. Daming Wang's contribution to this work is part-funded by the EU funded MaRINET 2 project (grant agreement ID:731084) and the School of Engineering, Computing and Mathematics at the University of Plymouth.

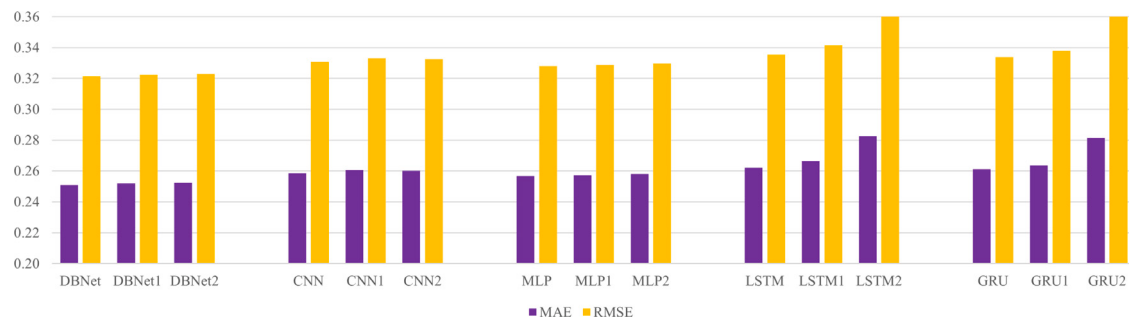


Fig. 12. The ablation study about the hyper-parameters of different machine learning methods used in our work.

References

- [1] Czech B, Bauer P. Wave energy converter concepts: Design challenges and classification. *IEEE Ind Electron Mag* 2012;6(2):4–16.
- [2] Rosa-Santos P, Taveira-Pinto F, Rodríguez CA, Ramos V, López M. The CECO wave energy converter: Recent developments. *Renew Energy* 2019;139:368–84.
- [3] Li G, Weiss G, Mueller M, Townley S, Belmont MR. Wave energy converter control by wave prediction and dynamic programming. *Renew Energy* 2012;48:392–403.
- [4] Zhan S, Li G. Linear optimal noncausal control of wave energy converters. *IEEE Trans Control Syst Technol* 2018;27(4):1526–36.
- [5] Zhang Y, Li G. Non-causal linear optimal control of wave energy converters with enhanced robustness by sliding mode control. *IEEE Trans Sustain Energy* 2019;11(4):2201–9.
- [6] Zhang Y, Stansby P, Li G. Non-causal linear optimal control with adaptive sliding mode observer for multi-body wave energy converters. *IEEE Trans Sustain Energy* 2020;12(1):568–77.
- [7] Liao Z, Gai N, Stansby P, Li G. Linear non-causal optimal control of an attenuator type wave energy converter m4. *IEEE Trans Sustain Energy* 2019;11(3):1278–86.
- [8] Ling BA, Bosma B, Brekkein TK. Experimental validation of model predictive control applied to the Azura wave energy converter. *IEEE Trans Sustain Energy* 2019;11(4):2284–93.
- [9] Ringwood JV, Bacelli G, Fusco F. Energy-maximizing control of wave-energy converters: The development of control system technology to optimize their operation. *IEEE Control Syst Mag* 2014;34(5):30–55.
- [10] Falnes J. Optimum control of oscillation of wave-energy converters. In: The eleventh international offshore and polar engineering conference. OnePetro; 2001.
- [11] Nguyen H-N, Tona P. Short-term wave force prediction for wave energy converter control. *Control Eng Pract* 2018;75:26–37.
- [12] Nguyen H-N, Tona P. Wave excitation force estimation for wave energy converters of the point-absorber type. *IEEE Trans Control Syst Technol* 2017;26(6):2173–81.
- [13] Hlope T, Wolgamot H, Taylor PH, Kurniawan A, Orszaghova J, Draper S. Wave-by-wave prediction in weakly nonlinear and narrowly spread seas using fixed-point surface-elevation time histories. *Appl Ocean Res* 2022;122:103112.
- [14] Tolman HL, et al. User manual and system documentation of WAVEWATCH III TM version 3.14. Tech Note MMAB Contrib 2009;276(220).
- [15] Booij N, Ris RC, Holthuijsen LH. A third-generation wave model for coastal regions: 1. Model description and validation. *J Geophys Res: Oceans* 1999;104(C4):7649–66.
- [16] Group TW. The WAM model—A third generation ocean wave prediction model. *J Phys Oceanogr* 1988;18(12):1775–810.
- [17] Law Y, Santo H, Lim K, Chan E. Deterministic wave prediction for unidirectional sea-states in real-time using artificial neural network. *Ocean Eng* 2020;195:106722.
- [18] Duan W, Ma X, Huang L, Liu Y, Duan S. Phase-resolved wave prediction model for long-crest waves based on machine learning. *Comput Methods Appl Mech Engng* 2020;372:113350.
- [19] Mohaghegh F, Murthy J, Alam M-R. Rapid phase-resolved prediction of nonlinear dispersive waves using machine learning. *Appl Ocean Res* 2021;117:102920.
- [20] Fusco F, Ringwood JV. A study of the prediction requirements in real-time control of wave energy converters. *IEEE Trans Sustain Energy* 2011;3(1):176–84.
- [21] Sheng W. Wave energy conversion and hydrodynamics modelling technologies: A review. *Renew Sustain Energy Rev* 2019;109:482–98.
- [22] Wijaya AP, Naaïjen P, van Groesen E, et al. Reconstruction and future prediction of the sea surface from radar observations. *Ocean Eng* 2015;106:261–70.
- [23] Ruban VP. Predictability of the appearance of anomalous waves at sufficiently small Benjamin–Feir indices. *JETP Lett* 2016;103(9):568–72.
- [24] Wang G, Pan Y. Phase-resolved ocean wave forecast with ensemble-based data assimilation. *J Fluid Mech* 2021;918.
- [25] Qi Y, Wu G, Liu Y, Kim M-H, Yue DK. Nonlinear phase-resolved reconstruction of irregular water waves. *J Fluid Mech* 2018;838:544–72.
- [26] Wang G, Zhang J, Ma Y, Zhang Q, Li Z, Pan Y. Phase-resolved ocean wave forecast with simultaneous current estimation through data assimilation. *J Fluid Mech* 2022;949:A31.
- [27] Simanesew A, Trulsen K, Krogstad HE, Borge JCN. Surface wave predictions in weakly nonlinear directional seas. *Appl Ocean Res* 2017;65:79–89.
- [28] Cousins W, Onorato M, Chabchoub A, Sapsis TP. Predicting ocean rogue waves from point measurements: An experimental study for unidirectional waves. *Phys Rev E* 2019;99(3):032201.
- [29] Fan S, Xiao N, Dong S. A novel model to predict significant wave height based on long short-term memory network. *Ocean Eng* 2020;205:107298.
- [30] Gracia S, Olivito J, Resano J, Martin-del Brio B, de Alfonso M, Álvarez E. Improving accuracy on wave height estimation through machine learning techniques. *Ocean Eng* 2021;236:108699.
- [31] Kumar NK, Savitha R, Al Mamun A. Ocean wave height prediction using ensemble of extreme learning machine. *Neurocomputing* 2018;277:12–20.
- [32] Jain P, Deo M, Latha G, Rajendran V. Real time wave forecasting using wind time history and numerical model. *Ocean Model* 2011;36(1–2):26–39.
- [33] Wang N, Chen Q, Zhu L, Sun H. Integration of data-driven and physics-based modeling of wind waves in a shallow estuary. *Ocean Model* 2022;172:101978.
- [34] Wu M, Stefanakos C, Gao Z. Multi-step-ahead forecasting of wave conditions based on a physics-based machine learning (PBML) model for marine operations. *J Mar Sci Eng* 2020;8(12):992.
- [35] Domala V, Lee W, Kim T-w. Wave data prediction with optimized machine learning and deep learning techniques. *J Comput Des Eng* 9(3).
- [36] Ma X, Huang L, Duan W, Jing Y, Zheng Q. The performance and optimization of ANN-WP model under unknown sea states. *Ocean Eng* 2021;239:109858.
- [37] Ma Y, Sclavounos PD, Cross-Whiter J, Arora D. Wave forecast and its application to the optimal control of offshore floating wind turbine for load mitigation. *Renew Energy* 2018;128:163–76.
- [38] Zhang J, Zhao X, Jin S, Greaves D. Phase-resolved real-time ocean wave prediction with quantified uncertainty based on variational Bayesian machine learning. *Appl Energy* 2022;324:119711.
- [39] Le Quang T, Dao MH, Lu X. Prediction of near-field uni-directional and multi-directional random waves from far-field measurements with artificial neural networks. *Ocean Eng* 2023;278:114307.
- [40] Marsaleix P, Michaud H, Estournel C. 3D phase-resolved wave modelling with a non-hydrostatic ocean circulation model. *Ocean Model* 2019;136:28–50.
- [41] Pirhooshyaran M, Snyder LV. Forecasting, hindcasting and feature selection of ocean waves via recurrent and sequence-to-sequence networks. *Ocean Eng* 2020;207:107424.
- [42] Gehring J, Auli M, Grangier D, Yarats D, Dauphin YN. Convolutional sequence to sequence learning. In: International conference on machine learning. PMLR; 2017, p. 1243–52.
- [43] Hochreiter S, Schmidhuber J. Long short-term memory. *Neural Comput* 1997;9(8):1735–80.
- [44] Cho K, van Merriënboer B, Bahdanau D, Bengio Y. On the properties of neural machine translation: Encoder–decoder approaches. In: Proceedings of SSST-8, eighth workshop on syntax, semantics and structure in statistical translation. 2014, p. 103–11.
- [45] Qi Y, Wu G, Liu Y, Yue DK. Predictable zone for phase-resolved reconstruction and forecast of irregular waves. *Wave Motion* 2018;77:195–213.